Received: 20 September 2022 | Revised: 20 August 2023 | Accepted: 17 September 2023

IET Image Processing

DOI: 10.1049/ipr2.12937

The Institution of Engineering and Technology WILEY

ORIGINAL RESEARCH

A robust watermarking approach against high-density salt and pepper noise (RWSPN) to enhance medical image security

Javad Ebrahimnejad[1] | **Alireza Naghsh**[1,2] | **Hossein Pourghasem**[1,2]

[1]Department of Electrical Engineering, Najafabad Branch, Islamic Azad University, Najafabad, Iran

[2]Digital Processing and Machine Vision Research Center, Najafabad Branch, Islamic Azad University, Najafabad, Iran

Correspondence
Alireza Naghsh, Department of Electrical Engineering, Najafabad Branch, Islamic Azad University, Najafabad, Iran.
Email: naghsh.a@pel.iaun.ac.ir; naghsh.a@gmail.com

Abstract

This paper proposes a robust watermarking method against high-density salt and pepper noise attacks. Automatic region of interest (ROI) detection, embedding encoded data, removing different densities of noise, data extraction by omitting, and labeling the noisy pixels of Region of Non-Interest (RONI), and decoding the extracted data using ROI pixel information as a key, are various steps of the presented scheme. The automatic ROI detection method separates the RONI from ROI with four vertices of the smallest rectangle, for the embedding process. The encoded watermark data is embedded into the least significant bits of RONI in four neighbour pixels. Adaptive Removal of high-density Salt and pepper Noise method can enhance image quality and reduce the effect of salt and pepper noise attacks. The embedded information is preserved from destruction if the host image is impaired through the power of robustness. The best results are obtained through the action of extracting the watermark from RONI pixels, utilizing the same ROI detection method. Omitting and labeling the noisy pixels of the RONI will ensure healthy extracted watermark data, leading to decreased Bit Error Rate (BER) values. Finally, these data are interpreted using the key of ROI pixels, and the watermark data is decoded and retrieved. Due to salt and pepper noise obliterating pixel bits and their corresponding transform coefficients in the transform domain, the spatial domain is employed to enhance robustness against such attacks. The results show the high performance of the presented scheme. The average BER value for five MRI databases in a 97% salt and pepper noise attack is 38.6.

1 | INTRODUCTION

In recent years, the extensive usage of digital data, especially in remote applications, and the significant advancement of the Internet of Things (IoT) in healthcare systems have caused the mishandling and tampering of the original content [1–3]. To this end, researchers have developed various digital watermarking methods in this field over the past years [4]. Medical image watermarking has many practical applications in telemedicine and related subjects. The exchange of medical images between specialists and hospitals provides a platform for discussion and diagnostic and therapeutic consultation. For this purpose, the electronic patient records (EPR), which contain medical and identification information of patients, and the related medical images are sent to the destination. Using different watermarking methods and integrating the EPR in medical images guarantees medical images' confidentiality, security, accuracy, and integrity [1, 5, 6]. In addition, authentication and tampering detection methods can be used to identify the source of medical images and determine the manipulation's location. The region of interest (ROI) in medical images is essential for diagnosis and should be protected. Then, authentication and retrieval information are embedded in some image blocks' pixels to obtain the watermarked image. By extracting the authentication information, tamper detection of the watermarked image has been determined. When the significant area is manipulated, the altered area can be automatically identified. The original image of the ROI is reconstructed with an invisible and low distortion [1, 7]. The authentication of medical images using watermarking methods has become a ubiquitous field of research, and many

reports have been published in this field. Furthermore, many data-hiding schemes have been proposed to hide patient data in medical images to reduce capacity, storage costs, and transfer time.

1.1 | Contribution

Maintaining an unaltered ROI in medical diagnosis is crucial for an infinite PSNR (Peak Signal to Noise Ratio), as highlighted in the article. The study focuses on maintaining security through ROI-based embedding and extraction. The research centers on labeling healthy/unhealthy pixels and data interpretation for recovery. Extracting data from healthy pixels in the RONI (Region of Non-Interest) area can reduce noise, lower BER, and protect medical watermark data in telemedicine. The transform domain is commonly used for image robustness, but it has two downsides: low data embedding capacity and vulnerability to certain attacks (e.g. salt and pepper noise, speckle, and cut) even at low densities that ruin pixel bits and transform coefficients. Transform domain methods can be affected when a single pixel is changed.

That is why we investigate and use the robustness in the spatial domain instead of the transform domain in this research. This research focuses on salt and pepper noise as an attack that can be intentional or unintentional. Although the probability of salt and pepper noise with a density of 97% is low, in practice, it can destroy the entire data as an intentional attack. The new idea presented in this article makes it possible to reconstruct the image with an acceptable PSNR, even in very high densities where almost the entire image is destroyed and only 3% of pixels are healthy. In addition, the results of low BER also show data recovery at an acceptable level.

2 | RELATED WORKS

There are several methods of watermarking in transform and spatial domains, each of which has advantages and disadvantages. Some of the previous works and their pros and cons are presented in the following.

The evolutionary cuckoo search algorithm has been introduced to obtain the optimal scale coefficients and improve the robustness and invisibility of watermarks in digital image watermarking [8]. For the robustness evaluation of the proposed method, several geometric and signal processing attacks are applied to the watermarked image. Analysis of experimental results shows the efficiency of the proposed method. The requirements of capacity, strength, invisibility, and security for proper watermarking are met in this method. The PSNR value increases compared with the discrete wavelet transform (DWT), indicating a better quality in the watermarked image. The article [9] presents a method for watermarking two separate digital signals in six bits of salt and pepper noise applied to a digital image. Because the salt and pepper noise is randomly distributed throughout the image, the pixel information of two separate images can be embedded in this noise. Then the embedded noise information is extracted into other applications, and the noise will be removed from these three images. The research in reference [10] provides an improved watermarking algorithm by hybrid usage of DWT, discrete cosine transform (DCT), and singular value decomposition (SVD). Arnold's transform scrambles the watermark image, and then this tangled image is transformed by DCT and SVD. The robustness of this algorithm is increased using encryption on the watermarked image, which leads to its compression. Experimental results show that the proposed technique is robust to all types of salt and pepper attacks, Gaussian noise, Joint Photographic Experts Group (JPEG) compression, cropping, rotation, scale, sharpening mask, histogram, and Poisson attack. The combination of DWT, DCT, and SVD was used in [11] to create a robust hybrid multiple watermarking method. Multiple watermarks are simultaneously embedded into the same medical image to provide more security and performance. The encryption method before embedding is used to enhance EPR security. Changing the gain factor, size of the text watermark, and cover images show high robustness, capacity, and reduced storage and bandwidth requirements. Reference [12] proposes a watermarking scheme for patient data, combining DCT and SVD to embed a secret logo in the coefficients of the transform domain. The chaos encryption increases the security of the watermark before embedding. The results of some signal processing and geometrical attacks show the very high robustness of the watermark. The study in [13] presents a fragile watermarking method for tamper detection and localization of medical and general images. The cover image is partitioned into non-overlapping blocks called Upper Half Block (UHB) and Lower Half Block (LHB). The embedded data in LHB are for tamper detection, and the ones in UHB are for tamper localization. Results show the capability of tamper detection and localization, high visual quality, and low computational complexity. A region-based multiple watermarking Firefly optimized algorithm with DWT and Schur transforms is proposed in the article [14] to support security issues of medical images during an interchange in telemedicine applications. The authenticity is delivered by embedding multiple robust watermarks in the RONI using a blind technique in the DWT-Schur transform. Simulation results show the performance of the launched algorithm in offering essential security benefits in telemedicine.

A combination of multi-level DCT, DWT, and SVD as a digital watermarking scheme is proposed in [15]. The Arnold transform is used to encrypt the watermark and improve security. The robustness evaluation of the proposed plan is done in the presence of different attacks, and its performance is measured with the normalized correlation (NC) and PSNR parameters. A new method in medical image applications, based on fragile watermarking for authentication and self-recovery, is proposed in the paper [16]. This method detects image manipulation and also retrieves the original image. The insertion of the self-recovery bit is determined using the Arnold transform. The proposed design is robust to various attacks, such as text deletion, text insertion, and copy and paste. The proposed research in reference [17] focuses on the precise extraction of patient data from medical images in the presence of salt and pepper noise,

which uses a data encryption method based on Reed Solomon error control encoding. Instead of the classic bit replacement methods for data hiding, the direct embedding of a symbol in pixel brightness is used. This method has a higher embedding capacity and increases the robustness against salt and pepper noise. Experimental studies on X-ray images, CT, ultrasonic, and MRI show that the watermark data are extracted more accurately from the watermarked images (stego images) in different salt and pepper noise densities. The PSNR of watermarked images is between 35 and 52 dB, inversely related to embedding capacity. The BER for noise density between 0% and 10% is less than 1%, and for 20% noise density, it is between 3% and 4% and above 20%, is significantly increased and reaches above 25%. Also, the BER is low against Gaussian and uniform noise attacks but high for speckle noise. A two-level data encoding process is proposed in [18] for reversible data hiding using dual stego-images. For obtaining the dual stego-images, the folded intensities are embedded in the cover image. This scheme reduces the intensity of hidden data; therefore, the quality of the two stego-images increases. This approach increases the PSNR near 2 dB and embedding rate (bpp) by 1%. The approach in [19] proposed a secure neural network-based watermarking technique for digital images. The LSB is used to insert a watermark and an Artificial Application Neural Network (ANN) for detecting and extracting sensitive information from the source image. Reversible watermarking is an area of active research in data security. In the article [20], reversible watermarking transfers the EPR and medical image authentication. In this method, an adaptive authentication code is obtained from the image to be watermarked. The watermark data embedding is done with the help of the innovative operation of increasing the scale of the original image. The results of applying this method to medical image databases in the presence of some conventional and geometric attacks show the highest PSNR as well as structural similarity (SSIM). The study [21] presents a reversible watermarking method using integer wavelet transform (IWT) in each iteration for embedding one watermark bit in one transform coefficient. The low distortion rate is achieved by the distortion compensation method. The result of the proposed method shows the watermarking approach's high capacity and low distortion.

A new way of medical image watermarking in the DCT domain using the 'Advanced Encryption Standard (AES)' algorithm has been proposed in [22]. The patient data is embedded in the relevant medical image. The encryption is done based on the chaotic technique to increase the robustness of watermarked images. The turbo serial code was used to retrieve the embedded information to control identification after the attacks. Experiments revealed a strong average PSNR and robustness against different attacks (compression, Gaussian noise, middle filter, crop, and rotation). An IWT-LSB watermarking scheme as a security system for medical image transmission is presented in [23]. The encryption based on random permutation and chaos is done for more confidentiality, integrity, authentication, and nonrepudiation of medical images. Experimental results show the high security of the method against different forms of attacks. Two different transform domain watermarking techniques for medical images are used [24]. The first is embedding a digital watermark and EPR into ROI and RONI. In the second approach, the digital watermark and EPR are embedded only into the RONI, and the ROI did not change for the telediagnosis goals. In both methods, the 8×8 block-based DCT was used. The proposed techniques are robust against singular and hybrid attacks. For medical image encryption, a new simple chaotic system using a decorrelation operation and a hyperbolic sinus is presented in [25]. The results indicate this scheme can encrypt images in a single round and increases security against common attacks. A new blind solution for medical images is proposed for invisible and secure watermarking based on the Schur analysis and chaos sequence method [26]. This scheme applies a chaos-based method to the watermark and the host image to split the encrypted images into sub-blocks. Schur-based decomposition is used to embed encrypted watermark bits in host image blocks. The same chaos sequence is used to extract the original watermark. The test results show high image strength and fidelity. The study [27] combines the optimization framework and DWT for watermarking. The watermark image is split into several blocks, and the proper location for each block is found in the cover image using the differential evolution (DE) method. These locations are embedded in the cover image of the wavelet domain used for reconstruction. Several experiments illustrate the algorithm's high imperceptibility and robustness against different attacks. The IoT-based healthcare system's privacy and data security problems are discussed in [28]. A robust method based on federal learning called Zero-watermarking is used to avoid skin medical image tampering and non-disclosure of health care data in which the watermark is not embedded in the image. The proposed method does not change important information in medical images and does not disclose data privacy. Experimental results show that the proposed scheme is more robust to conventional and geometric attacks and performs better than other zero-watermarking methods. To maintain the quality of the medical image, reference [29] presents an adaptive reversible watermarking algorithm in which the medical image characteristics are supposed. This algorithm is used based on an estimated error expansion procedure during object and background region segmentation. Expanding the estimated error from neighbouring pixels embeds the patient information or a hash code as a watermark. By watermark extraction, the original image is reconstructed with no quality degradation. The proposed algorithm performed well in capacity, perceptual quality, and reconstruction rate.

Although transform domain watermarking methods are robust against attacks, they have lower capacity and more complexity. On the contrary, spatial domain methods have higher capacity and less robustness against attacks. This research studied transform domain watermarking at the [8, 10–12, 14–16, 21–23, 24, 27, 28], which contains DWT, IWT, SVD, DCT, and some combinations of them with other intelligent and heuristic methods. The downsides of these methods are low embedding capacity and less robustness against salt and pepper noise (especially for high-density). Also, the spatial domain watermarking techniques investigated in [13, 17–20, 25, 26, 29-31] use directly the LSB or most significant bit (MSB) bits of pixels

and some combinations with artificial intelligence and encryption methods. The disadvantages of these schemes are that they are not robust against attacks and have low PSNR. The new approach proposed in this research provides the advantage of the transform domain (robustness) and the advantage of the spatial domain (high capacity) simultaneously. According to the mentioned methods and requirements, image quality and data security are crucial since medical image applications and remote access have increased. Therefore, errors in data recovery and image reconstruction problems cause the doctor's incorrect diagnosis. Also, these lead to the disclosure of patient information and authentication issues in accessing medical images. Improving the parameters and criteria mentioned in the above records can prevent loss of life and property. Therefore, due to the breadth of criteria and their combination, there are vast fields for research and innovation in medical image watermarking. The main issue of the present study is the complete retrieval of the watermarked data, which includes EPR and any other valuable data from the physician's point of view, in the presence of intentional salt and pepper noise attack (especially with high density) or transmission media noise, and the reducing the BER value near to zero. In addition, promoting the visual quality of the original image after removing the noise and extracting the data, and helping the doctor to diagnose the disease truly, will be done. The presence of noise with a density of 97% may not occur in practice for the whole image. However, even if a small part of the image is noisy because of an intentional or non-intentional attack in a short time, in milliseconds, it can be removed by the adaptive removal of the high-density salt and pepper noise (ARSPN) method. In the following, the proposed method of data watermarking process in an MRI medical image and then retrieval and decoding of this data is presented. Finally, the evaluation of the proposed scheme with BER, PSNR, and SSIM criteria is examined.

3 | PROPOSED METHOD

3.1 | Watermark encoding and embedding procedure

Before beginning the watermarking process, isolating the ROI with an automatic solution is necessary for the watermark data embedding in the RONI. The automated area identification procedure contains the following steps: morphological reconstruction of the incoming medical image, applying a Gaussian low-pass filter in the frequency space, thresholding and filling cavities, labelling, and finding the biggest area, defining the largest region boundary, and finally, the separation of the ROI in a rectangle [31]. As a preprocessing part of the proposed method, the opening morphology filter increases identification accuracy by removing small pieces and modifying the main parts of medical images. In the case of low-quality images, a Gaussian filtering step for attenuating the frequency components farther from the centre of the image is required to ensure complete detection of the critical area. In the proposed method, *greythresh* automatic function of the Matlab software is used for thresholding. In addition, for each database, a specific coefficient is multiplied by the calculated threshold value. This coefficient is obtained experimentally, and the accuracy of the binarization process increases. The coefficient obtained in this paper is between 0.2 to 0.5. Since the thresholding stage may remove some parts of the ROI, some holes and discontinuities appear in the binary image, so the morphological closing operation fills these holes. As the last step, the labelling method removes unwanted areas. The largest area is obtained by labelling and classifying the marked objects based on their size. As a result, the ROI is segmented by selecting the biggest connected components of the labelled image. The area border is determined by changing its pixel colour when selecting the biggest area. The segmented ROI is presented inside the main image in green by replacing the binary image with the original one. Finally, in Figure 1, the segmented ROI is shown in a rectangle [31].

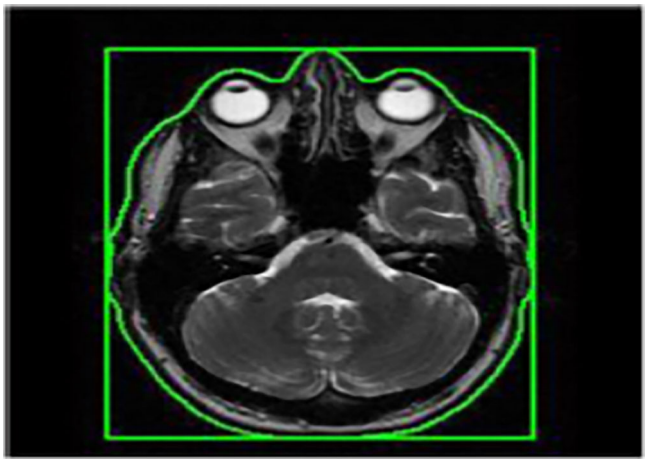

FIGURE 1 The ROI segmented in a rectangle. ROI, region of interest [31].

Another step is added to the above process to increase the robustness of identifying the ROI and comparative accuracy (CA). The extracted ROI has a rectangular shape in the previous steps, with four points at its corners. These points are changed with the correction parameter (C_p) between 5 and 25, in a way that remains unchanged against attacks such as average, median, wiener, Gaussian, sharpening, moving filters, and speckle noise. This method of changing points is called window size correction (WSC). Figure 2 shows two different scales of the identified ROI (with dotted line) that the points of these two areas are transferred by the WSC method to new points, a'_i. The WSC produces the same points before and after the attack for the ROI [31]. The WSC method is implemented based on Equations (1) and (2).

$$a'_i = \begin{cases} a_i + k_1, & k_1 < \dfrac{C_p}{2} \\ a_i - k_0, & k_1 \geq \dfrac{C_p}{2} \end{cases} \tag{1}$$

$$\begin{cases} k_0 = mod(a_i, C_p) \\ k_1 = C_p - mod(a_i, C_p) \end{cases} \tag{2}$$

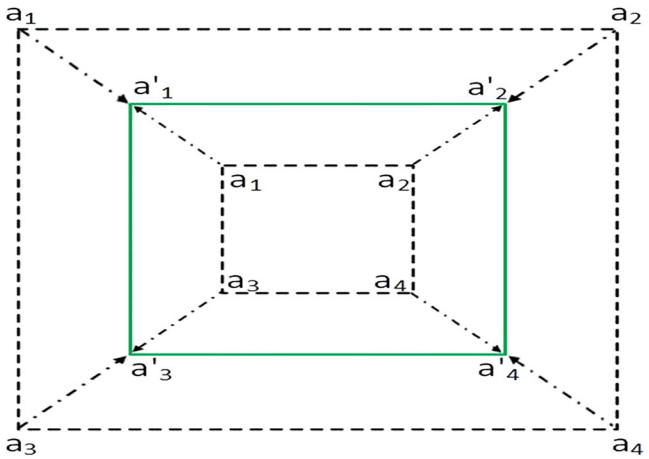

FIGURE 2 The window size correction method [31].

The different stages of robustness evaluation of the proposed process of identifying the ROI in the presence of attack and after WSC are as follows: first, the ROI of medical images with and without noise is selected through the proposed automatic method, and four vertices of each one are found. After that, the WSC modifies these points. Finally, the CA is calculated by comparing four vertices of selected ROI with and without noise. The high CA shows the same result of ROI selection before and after the noise attack. After separating the ROI, watermarking and embedding the data begins. The watermark production block in this paper includes three steps described as follows and shown in Figure 3 [31]:

Step 1: ROI partitioning: While the ROI is segmented, it is divided into several non-overlapping partitions, as shown in Figure 4.

Step 2: Binarizing and partitioning the EPR: One type of watermark data is the patient's electronic file, EPR, usually in 'n ASCII code. Two preprocessing steps are applied to prepare the EPR characters for embedding in RONI. The first one converts the entire ASCII code into a unique binary stream. The second one divides the generated binary stream equally by the number of ROI blocks (Figure 5). If any of the blocks are broken, only the EPR bits belonging to the same block will be affected.

Step 3: Encrypting the partitioned and binarized EPR: To encrypt the EPR data according to the previous two steps, each bit of every block of the binary and partitioned file with bits number 9, 10, and 11 of the corresponding block in the partition ROI is compared, and a two-bit code is generated for this comparison. If a bit of patient data is equal to bit nine of ROI pixel, the 01 code is generated, and if it is the same as bit number 10, the 10 code is considered. If the desired bit of patient data is equal to the eleventh bit of the corresponding pixel in the ROI, the 11 code is generated, and if it is not equal to any of the three bits, the 00 code is considered.

The length of the address generated after encrypting a bit of the EPR ($L_{\text{EPR\_Encod}}$) is twice the number of ROI pixels used in the encryption. Each binary bit of the EPR can be encrypted by more than one pixel of the ROI to increase accuracy during the decryption process. This paper uses four neighbourhood ROI pixels in a 2 ×2 window to encrypt each binary bit of the EPR data. By encrypting each bit with four ROI pixels, the encrypted bit of EPR can still be recovered if there are even small changes in the used ROI pixels. The number of watermark bits generated after encrypting all the EPR bits ($N_{\text{Gen\_Wat}}$) is shown in Equation (3):

$$N_{Gen\_Wat} = N_{EPR\_Char} \times a \times L_{EPR\_Encod} \tag{3}$$

where $N_{\text{EPR\_Char}}$ is the number of characters in the EPR, a is the numeric coefficient to convert the ASCII code to binary format ($a = 8$).

The RONI pixels are used for the watermark bits embedding after generating the encrypted sequence from all the EPR bits. The bits number per pixel for all images is 16, and the image dimensions are M × M. The embedding process starts from the top-left corner pixel and continues from right to left and top to bottom. To insert the EPR data into the RONI pixels, the pixels' number in this region is first calculated in Equation (4).

$$N_{RONI\_pixel} = N_{Total\_pixel} - N_{ROI\_pixel} \tag{4}$$

The maximum embedding capacity is obtained in the next step based on Equation (5). This capacity depends on the RONI bits number per pixel used for embedding (embedding depth). Increasing the depth increases the embedding capacity in the RONI, reducing the visual quality, reducing the error rate, and making the embedded information more visible.

$$C_{Max\_RONI} = N_{RONI\_pixel} \times E_{depth} \tag{5}$$

In the proposed method, the embedding depth is four, that is, four less significant bits of each pixel in the RONI are used to hide the watermark bits, as shown in Figure 6.

The PSNR and SSIM criteria for the watermarked image depend on the number of bits embedded in the RONI, based on Equations (6) and (7) ($N_{\text{EMB\_bits}}$).

$$N_{EMB\_bits} = N_{Gen\_Wat} \times N_{Repetition} \tag{6}$$

$$N_{EMB\_bits} \le C_{Max_{RONI}} \tag{7}$$

The next stage of embedding involves the embedding strategy. It means that the generated watermark data is hidden inside the pixels of the RONI. For this purpose, a binary bit of the EPR data is considered. After encrypting this bit with four pixels of the ROI, an eight-bit code is generated. The two least significant bits (bits 1 and 2) of RONI, located in a 2 × 2 window, will be the place for embedding these eight bits. The watermark extraction process must also maintain this embedding order. According to Figure 7a, the first two least significant

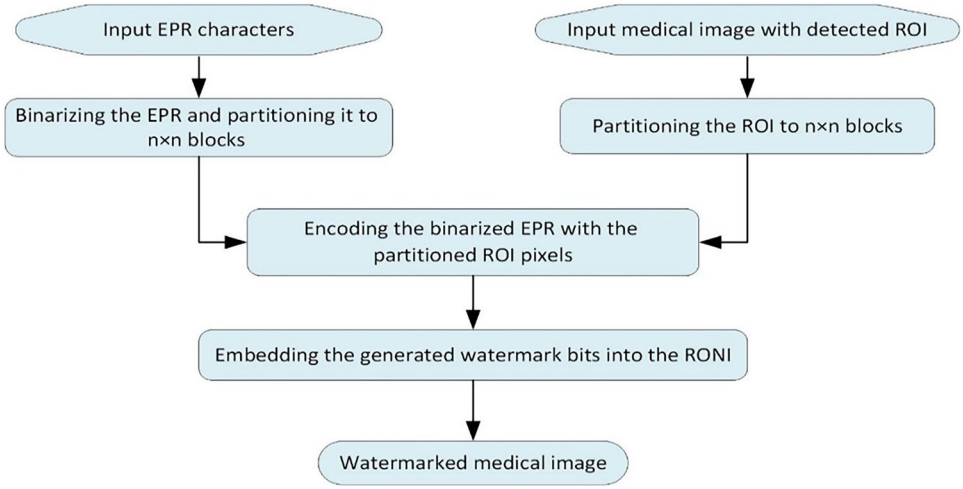

FIGURE 3 Overview of the proposed watermarking process [31].

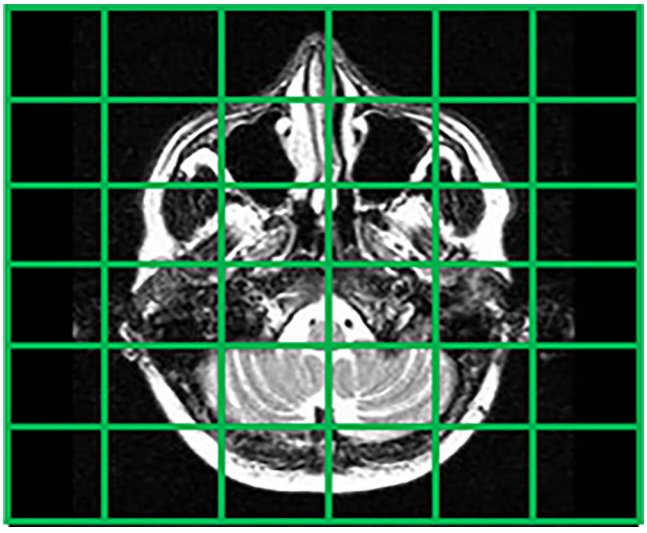

FIGURE 4 The partitioned ROI in 6 × 6 blocks. ROI, region of interest [31].

0111	1110	0010	1100	1111	0101
1010	0011	0110	0010	0010	0110
1100	1110	0010	0111	1110	0010
0110	1100	0010	0111	0110	1100
0111	1110	0000	1100	0111	1110
0111	1010	1100	0110	0000	0000

FIGURE 5 The partitioned EPR in 6 × 6 blocks. EPR, electronic patient records [31].

bits in each neighborhood of the RONI pixels create a 2 × 2 × 2 cube inside the RONI to embed these eight bits. A simple attack which will be occurred to any watermarked image is the LSB removal attack. So, to increase the robustness of embedded watermark information and reduce error rate, another cube is used to repeat the same data in bits 1 and 2, using the third and fourth least significant bits of RONI pixels, and the process of the previous step is repeated precisely. This operation is shown in Figure 7b. Therefore, besides salt and pepper noise attack, the proposed method is robust against the LSB removal attack. After embedding all watermark bits, to increase the robustness of this data and reduce the error rate in retrieving them, all the above steps are repeated from the first watermark bit until there is enough space to embed in the RONI. The watermark recovery process involves several steps: salt

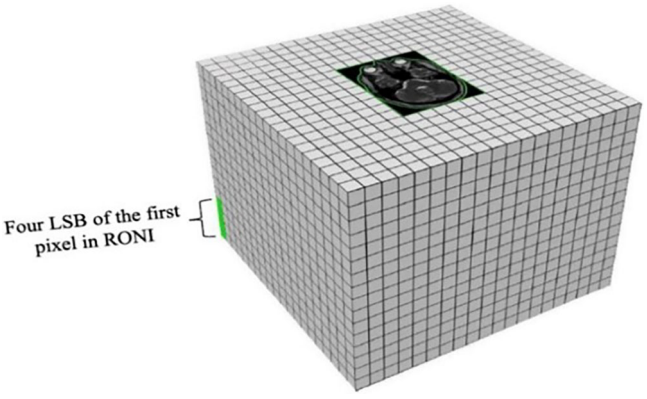

FIGURE 6 Embedding depth in RONI pixels. RONI, region of non-interest [31].

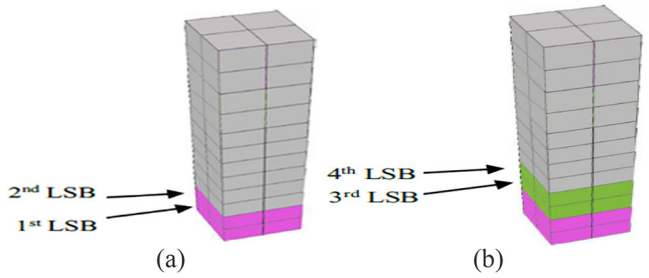

FIGURE 7 (a) Embedding the eight bits in the RONI cube. (b) Robustness of the embedding. RONI, region of non-interest [31].

and pepper noise cancellation by the Adaptive Removal of Salt and pepper Noise (ARSPN) [30] method, identifying the ROI, extracting the embedded data, and decoding it by the pixels of the ROI.

3.2 | Watermark data recovery procedure

After receiving the image at the destination, the noise removal block must first remove the noise added to the images to extract the watermark data. Afterwards, the ROI automatically identifies and selects the same as the embedding process. Then the embedded data in the RONI are extracted based on the embedding method. In the next step, the extracted data interpret and decoded based on the ROI as the key. Then, the robustness of embedded watermark bits against different densities of salt and pepper noise (1%–97%) is evaluated. For this purpose, the BER is obtained by extracting the embedded data and comparing it with the original data. The BER is calculated by assuming the repetition code for the embedding process in the presence of a noise removal block in the data extraction step. Comparing the mean BER of extracted watermark data in five databases and after the presence of salt and pepper noise attacks with different densities shows that the BER increases with increasing noise density. Also, comparing the results of the average PSNR and the SSIM criteria of the total watermarked images in five databases, after the presence of salt and pepper noise attack, before and after applying the noise removal block shows a significant increase in the values of these criteria after applying the ARSPN. The results show that the proposed method has high robustness to salt and pepper noise, and also, the presence of a noise removal block reduces the BER and improves the PSNR and the SSIM of the watermarked image. The scheme proposed in this article is better than all previous methods [31].

3.2.1 | Noise cancelation block (ARSPN)

According to this method, in the vicinity of each noisy pixel of the input image, an adaptive $n \times n$ window is considered—the value of n changes with the noise density. The noise-free pixels of this window will be weighed according to their distance from the desired pixel. The greater the distance, the less weight is added. The relationship between this weight and the distance is shown in Equation (8):

$$W(k) = 10^{-(k-1)}, \quad k = 1, 2, 3, 4, \ldots \tag{8}$$

where k is the distance between the window and desired pixel, and W is the desired weight. Then, the weighted sum of the adjacent pixels is averaged, and the resulting value replaces the noise pixel. The pseudo-code of the ARSPN approach is shown as Algorithm 1 in Figure 8 [30].

In this process, the desired window size is the first window size that contains healthy, noise-free pixels. It means that all low- and high-dimensional windows will be tested, and the first window with a healthy pixel will be the best window to eliminate noise at that density. A significant advantage of using this new method is removing high-density multimodal salt and pepper noise from a medical image. It means that if different densities of salt and pepper noise (in the range of 1%–97%) appear in an image, the new method can eliminate all of them based on density. In other words, if there is random noise anywhere in the image, this method only corrects the same noise area and leaves the rest of the image unchanged. Other previous methods affect the whole image and blur the healthy parts. The innovative approach is local [30]. Figure 9 shows the result of applying this method to some images.

3.2.2 | Watermark extraction and decoding

After de-noising the watermarked image with the ARSPN method and partitioning the detected ROI, the extraction and decoding process of encoded data starts with the reverse method of the embedding and encoding process. Watermark extraction from the RONI is done in two cases. The first case is the reverse process of the embedding method without any precondition; the embedded data is retrieved from the four least significant bits (bits numbers 1, 2, 3, 4) in the four neighbourhoods of each pixel. In the second case, the retrieval operation is performed only from pixels that are not noisy. If the pixels are noisy, a label is assigned instead of extracting the bit value of each pixel. After extracting the watermark data, the ROI key is used for interpreting and decoding it, and the extracted values are translated with bits numbers 9, 10, and 11 of each ROI pixel. For this purpose, two modes are considered. First, without any precondition, if two bits of the extracted data are equal to 01, the value of the recovered data is the same as the value of bit number nine of the corresponding ROI pixel. If these two bits are 10, the retrieved information is equivalent to the value of bit number 10, and if they are equal to 11, the decoded data is similar to the 11th bit of the corresponding pixel in the ROI. Therefore interpreting all extracted data is done by this method. In the second case, the extracted data bits are replaced by the value of bits numbers 9, 10, or 11 of each corresponding ROI pixel, provided that the ROI pixel is not noisy; otherwise, a label is assigned instead of the recovered and interpreted data.

Algorithm 1 . The pseudocode of the new method

```
Input = inputImage
output = filteredImage
for m = 1 : size(rows(Input)) do
    for n = 1 : size(columns(Input)) do
        d = distance between desired and window pixel
        if input(m, n) = S&Pnoise then
            for i = m − d : m + d do
                for j = n − d : n + d do
                    if input(i, j) ≠ S&P noise then
                        for k = 1 : d do
                            if k ≤ d then
                                W(k) = 10^−(k−1).
                                sum = sum + (input(i, j) × W(k).
                                count(k) = count(k) + 1.
                            else
                                d = d + 1.
                                continue
                            end if
                        end for
                    end if
                end for
            end for
        end if
        if W × count ≠ 0 then
            output = sum / W×count
        end if
    end for
end for
```

FIGURE 8 The pseudo-code of the ARSPN method. ARSPN, adaptive removal of high-density salt and pepper noise [30].

According to the above cases, four modes are considered in data recovery and evaluation of the used method and calculating the BER:

1. No-Labeled (no precondition for extraction and decoding)
2. ROI-Labeled (no precondition for extraction, but precondition for decoding)
3. RONI-Labeled (the precondition for extraction, but no precondition for decoding)
4. Both-Labeled (the precondition for extraction and decoding)

Figure 10 shows the algorithm diagram of the extraction and decoding procedure.

Finally, after labelling the noisy pixels in the extraction and interpreting steps, if the number of ones is more than 50% of total zeros and ones extracted and retrieved, the corresponding bit value for an encoded bit will be one; otherwise, it will be zero.

4 | EXPERIMENTAL RESULTS AND EVALUATION

Based on the above four modes to interpret the extracted data and innovative ARSPN solution, the methods mentioned are tested with five databases containing 181 MRI images. The BER factor is compared with previous approaches. Also, the results of PSNR value for different noise densities are discussed. The BER results obtained from applying the proposed method on database number 2 with 9 MRI images, in the presence of salt and pepper noise, up to a density of 97%, are shown in Table 1. It demonstrates that omitting the noisy pixels during extraction or interpretation affects the BER values differently by increasing the noise density. When the noisy pixels of ROI are omitted for interpretation (ROI-Labelled mode), the values of BER increase compared to the No-Labelled mode. The differences between the amounts of these two modes increase significantly for very high-density noise. It is because of destroying the pixels of ROI as the key, and the number of healthy pixels is very low for analyzing the values. By ignoring the noisy pixels of ROI and RONI together (Both-Labelled mode) for low- to medium-noise densities, the results of BER are better than the No-Labelled mode but growing the noise value leads to an increase in error, and the BER value is enhanced. This is because the number of healthy pixels is meager in the smallest window, supposed for the noise cancellation method, even if the window size increases. For noise densities from low to medium, ignoring only the noisy pixels of RONI decreases BER slowly, compared to the No-Labelled mode. But the results are unbelievable and amazing for high-density noises (more than 50%).

The results for Database no.2 (DB2) show that the case of RONI-Labelled has the best performance and outcomes. It means that, during the extraction process, if the RONI noisy pixels are ignored and labelled, only healthy data are extracted, and the BER is reduced. For a noise density of 95%, the average BER is 26.7, and for 97% of noise density, the BER is

TABLE 1 BER (%) results of applying the proposed method on DB2 in four modes.

Mode	Image No.	1%	5%	10%	20%	30%	40%	50%	60%	70%	80%	90%	95%	97%
No-Labeled	1	0	0.3713	0.37129	2.351485	4.579208	10.39604	20.42079	25.86634	29.57921	28.09406	43.19307	46.41089	38.86139
	2	0	0	0.12376	0.247525	4.331683	12.99505	19.55446	31.55941	33.78713	43.06931	41.08911	48.0198	47.27723
	3	0	0	0	0.742574	6.311881	7.178218	29.45545	33.29208	35.89109	36.38614	36.75743	39.35644	46.78218
	4	0	0	0.24752	0.866337	1.608911	19.18317	32.30198	38.4901	39.97525	43.19307	47.40099	50.12376	37.37624
	5	0	0.2475	0.37129	1.980198	7.054455	22.89604	30.32178	35.27228	37.25248	39.10891	39.60396	47.15347	39.72772
	6	0	0.1238	0.24752	0.742574	7.054455	19.80198	38.36634	42.82178	43.81188	43.81188	46.0396	45.91584	55.32178
	7	0	0	0.24752	0.990099	16.08911	22.77228	35.02475	37.37624	38.86139	37.62376	37.99505	39.10891	56.06436
	8	0	0	0	0	0.618812	9.405941	22.0297	28.09406	43.81188	39.60396	40.09901	28.09406	46.41089
	9	0	0	0.12376	0.371287	4.084158	33.78713	33.29208	35.27228	36.38614	52.9703	48.26733	56.18812	48.26733
Mode	**Image No.**	**1%**	**5%**	**10%**	**20%**	**30%**	**40%**	**50%**	**60%**	**70%**	**80%**	**90%**	**95%**	**97%**
Both-Labeled	1	0	0.247525	0.618812	2.59901	3.960396	9.034653	10.76733	19.92574	33.29208	56.06436	81.18812	92.82178	97.77228
	2	0	0.123762	0.247525	2.227723	4.950495	5.816832	12.5	17.94554	29.33168	50.74257	77.35149	92.07921	98.26733
	3	0	0.123762	0.618812	1.732673	2.846535	8.168317	14.10891	16.70792	29.9505	49.13366	79.08416	94.30693	97.27723
	4	0	0	0.742574	1.608911	3.217822	7.549505	6.806931	17.94554	28.58911	51.23762	77.84653	92.4505	97.89604
	5	0	0	0.247525	1.608911	2.970297	7.79703	13.36634	16.70792	29.57921	48.76238	74.87624	91.21287	95.54455
	6	0	0	0.618812	1.608911	3.217822	7.30198	10.5198	15.59406	27.47525	44.43069	73.63861	89.97525	96.65842
	7	0.247525	0	1.237624	2.970297	4.331683	7.178218	14.72772	18.93564	28.58911	51.85644	76.36139	91.08911	95.42079
	8	0.123762	0.123762	0.618812	2.475248	5.321782	8.292079	16.21287	20.0495	31.06436	51.36139	74.0099	92.20297	96.78218
	9	0	0.123762	0.371287	1.732673	2.722772	7.79703	12.99505	17.57426	27.47525	49.87624	75.49505	89.60396	95.79208
Mode	**Image No.**	**1%**	**5%**	**10%**	**20%**	**30%**	**40%**	**50%**	**60%**	**70%**	**80%**	**90%**	**95%**	**97%**
ROI-labeled	1	0	0.6188	0.86634	6.311881	9.158416	20.79208	27.47525	40.34653	49.75248	59.90099	75.37129	86.75743	88.98515
	2	0	0.1238	0.61881	2.10396	11.5099	19.43069	28.83663	43.68812	49.25743	61.5099	76.9802	90.34653	93.06931
	3	0	0	0.37129	2.846535	16.58416	18.31683	36.63366	45.54455	56.06436	58.29208	76.36139	88.73762	91.95545
	4	0	0	0.12376	1.608911	7.920792	26.48515	35.5198	48.14356	56.43564	71.16337	80.81683	89.85149	91.08911
	5	0	0	1.60891	7.920792	19.80198	36.13861	42.94554	43.93564	54.08416	65.59406	78.34158	90.71782	93.44059
	6	0	0.1238	1.11386	4.331683	17.94554	32.42574	43.56436	51.73267	58.04455	64.23267	79.70297	89.97525	94.18317
	7	0	0.1238	1.60891	8.663366	33.91089	27.59901	42.32673	50.37129	55.19802	64.4802	79.45545	86.26238	92.69802
	8	0	0.1238	0.49505	2.722772	8.168317	29.82673	36.88119	42.69802	54.9505	66.95545	75.61881	85.14851	93.81188
	9	0	0.495	1.23762	5.693069	15.59406	40.96535	41.21287	46.41089	52.47525	68.06931	80.56931	88.86139	92.20297
Mode	**Image No.**	**1%**	**5%**	**10%**	**20%**	**30%**	**40%**	**50%**	**60%**	**70%**	**80%**	**90%**	**95%**	**97%**
RONI-Labeled	1	0	0.247525	0.371287	0.866337	1.856436	2.846535	6.559406	6.311881	7.549505	13.73762	22.89604	35.02475	54.57921
	2	0	0	0.123762	0.247525	0.990099	2.475248	3.094059	6.064356	8.415842	12.12871	17.07921	29.57921	42.82178
	3	0	0	0	0.49505	1.237624	2.351485	3.341584	3.960396	6.683168	9.034653	14.97525	27.22772	39.4802
	4	0	0	0	0.618812	1.361386	1.485149	2.227723	4.207921	4.331683	7.79703	14.10891	24.0099	44.55446
	5	0	0.123762	0.123762	0.247525	0.742574	0.990099	1.980198	3.217822	5.940594	9.158416	14.60396	22.40099	34.03465
	6	0	0.123762	0.247525	0	0.371287	1.113861	1.237624	4.331683	5.321782	7.549505	11.01485	18.44059	31.93069
	7	0	0	0.247525	0.618812	1.608911	3.217822	3.341584	5.074257	5.445545	10.5198	15.22277	24.75248	34.28218
	8	0	0.247525	0.123762	0.618812	1.361386	2.846535	3.836634	5.074257	7.178218	11.38614	18.56436	23.88614	35.27228
	9	0	0.123762	0.247525	0.123762	0.49505	1.113861	2.846535	3.836634	6.188119	12.5	16.4604	23.88614	31.68317

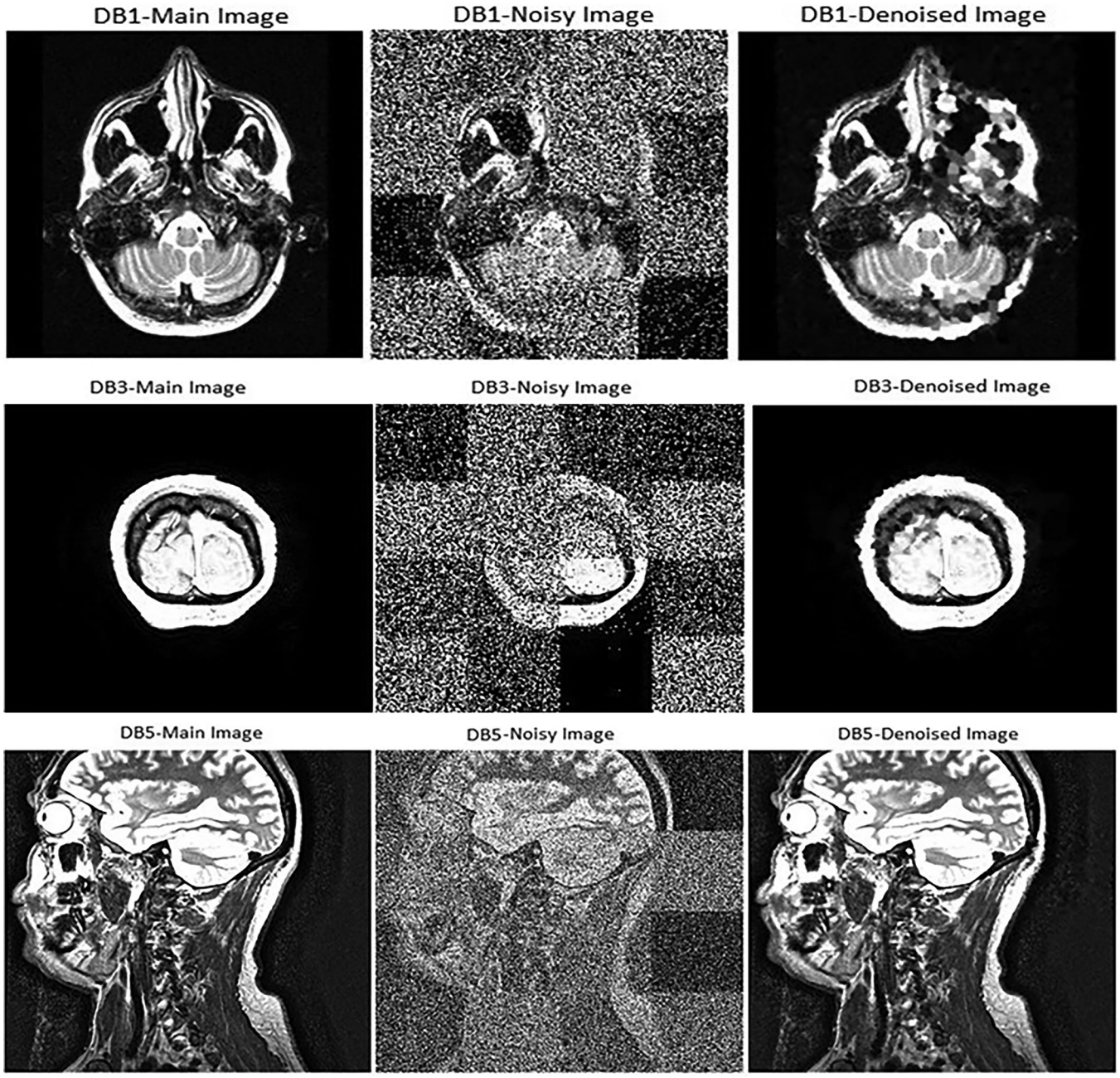

FIGURE 9 Result of applying ARSPN on some images. ARSPN, adaptive removal of high-density salt and pepper noise.

less than 40. This is because the noise destroys the bits of the pixels and changes their value entirely, and incorrect data are obtained in the recovery phase. Still, by ignoring the noisy pixels and using only the information of healthy pixels, the watermark data is extracted with a minimum error when interpreting and encoding them. The outcomes of other cases show that there is no need to label the noisy pixels of ROI during the decoding step. Since marking the ROI's noisy pixels may increase the whole labels during the decoding process and make a mistake in interpreting an encoded bit.

The BER average of applying the proposed method on each database in four modes, in the presence of different densities of salt and pepper noise, is displayed in Figure 11, which confirms the above explanation regarding Table 1. As it is clear in the results and the graph of Figure 11, for example, in the noise attack of 97%, the host image is only 3% healthy, while the watermarked information remains above 60% healthy. The first case is the same as the one presented in reference [31]. But because of using the ARSPN method, the BER results are better than this reference, especially for high-density noises. In the second case, since the extracted data from RONI did not get any label, the unhealthy pixel's information is interpreted with ROI healthy pixel's information. This comparison and interpretation of incorrect data with a beneficial key and reference cause more

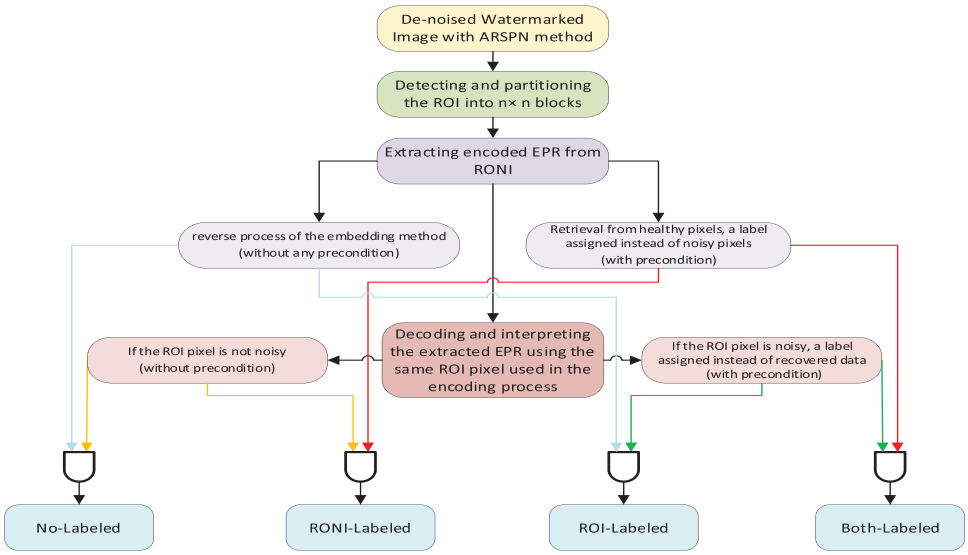

FIGURE 10 The algorithm diagram of the extraction and decoding procedure.

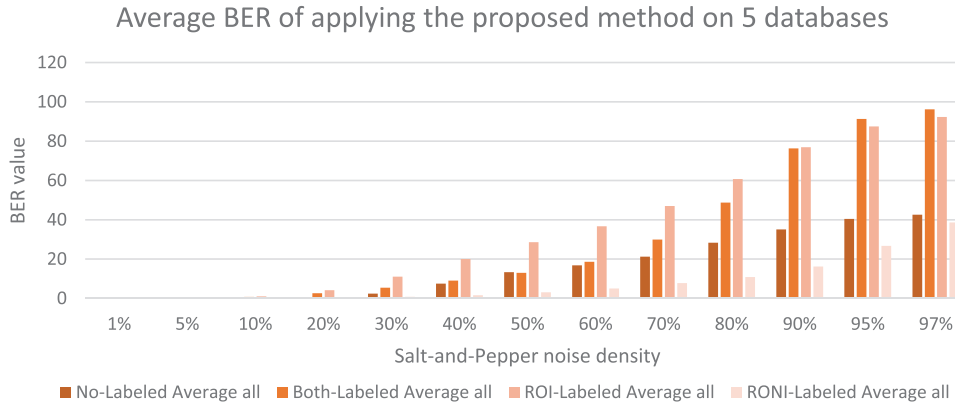

FIGURE 11 The BER (%) average of applying the proposed method to each database in four modes.

errors. Therefore, compared to the previous case, the results of this case are highly undesirable and unacceptable. In case number four, the healthy data of RONI pixels are interpreted by healthy data of ROI pixels. So, data from many pixels are ignored in the extraction and decoding stages (especially with increasing noise density). Therefore, the BER is very high due to a lack of data and has the worst results among the four cases. But in case number 3, since the data is extracted from healthy RONI pixels and then decoded using all ROI pixels' data as a key, the BER has the lowest results. Therefore, this is the best case for extracting and decoding the watermark data. The BER average value in the case of RONI-Labelled for very high-density noise (97%) is equal to 38.6 for all DBs.

By comparing the presented scheme with other related works and the [31], the high performance of this method is clearly shown in Table 2. Different combinations of watermarking methods with other techniques are applied. Also, various types of images participated in the experiments. Still, none of these references has efficient implementation and low BER in a wide range of salt and pepper noise attack, especially for high-density. It is evident in Table 2, the only method that, in addition to a sufficient number of images for testing, examines a wide range of noises and at the same time offers the benefits of spatial and transform domain watermarking and has a very low BER, the new method presented in this article.

On the other hand, the quality of the watermarked image after applying the noise removal method with different noise densities is measured by the PSNR criterion. It shows how much the quality of the watermarked image has changed after removing the noise and demonstrates the effectiveness of the noise removal method. Table 3 shows the results of PSNR on all DBs, in the presence of different noise densities up to 97%. These values indicate that although the noise density increases, due to the use of the ARSPN noise removal method, the quality of the denoised image is still acceptable, and the image is visible.

TABLE 2 Comparison between the proposed method and some other related works.

Reference	Method	Database	BER%
R. Sinhal et al. [32] (2021)	YCbCr colour space, IWT, DCT, ANN framework for colour image watermarking	Lena, Mandrill, Plane, Pepper, Sailboat, House, Barbara	Avg. for S&P 1 % = 0.023, Avg. for S&P 2 % = 0.1129, Avg. for S&P 5 % = 0.1024, Avg. of 34 attackes for 7 images with ANN = 0.0681
M. Z. Konyar and S. Öztürk [17] (2020)	Reed Solomon Coding-Based	36 images from European Society of Radiology database (CT, MRI, US, X-ray)	For S&P 50%: CT = 24.9, MRI = 25.1, US = 24.9, X-ray = 24.6
V. M. Manikandanm V. Masilamani [20] (2021)	Scaling-based reversible watermarking	1000 medical images-OsriX dataset	Avg. for S&P 1 % = 0.036, Avg. for S&P 5 % = 0.083, Avg. for S&P 10 % = 0.136, Avg. for other 10 attackes = 0.318,
A. Soualmi, et al. [26] (2021)	Schur triangulation and chaotic sequence	22 medical and non-medical images	Avg. for S&P 0.1 % = 0.001, Avg. for S&P 3 % = 0.004, Avg. for S&P 5 % = 0.008, Avg. for S&P 7 % = 0.011, Avg. for S&P 10 % = 0.016
S. M. Mousavi, et al. [31] (2017)	Spatial domain watermarking method, channel coding and noise filtering schemes	Five databases contain 179 MRI images	41.7 for 90% S&P noise density
Proposed method	ARSPN, automatic ROI detection, labeling the noisy pixels of RONI	171 MRI images	From 0% to 70% noise density: Avg. = under 10, from 80% to 95% noise density: Avg. = 10 to 26.7, for 97% noise density: Avg. = 38.6

Abbreviations: ANN, application neural network; ARSPN, adaptive removal of high-density salt and pepper noise; DCT, discrete cosine transform; IWT, integer wavelet transform; ROI, region of interest; RONI, region of non-interest.

TABLE 3 PSNR (dB) results of applying the proposed method on all DBs, for the salt and pepper noise attack from 1% to 97% density.

Noise	1%	5%	10%	20%	30%	40%	50%	60%	70%	80%	90%	93%	95%	97%
DB1	50.2206	43.2379	40.1538	36.9171	34.8320	33.1995	31.6238	30.1617	28.4852	26.7496	24.4603	23.4071	22.4529	21.4285
DB2	53.4390	46.2905	43.1005	39.9873	37.9326	36.3464	34.9091	33.3853	31.9425	30.3044	28.2016	27.0821	26.1641	25.3278
DB3	50.4264	43.3843	40.2635	37.0798	35.0363	33.4383	32.0164	30.6348	29.1561	27.5636	25.4911	24.4377	22.8738	21.4984
DB4	61.2648	54.0634	50.6892	47.1707	44.7840	42.7183	40.8027	38.8716	36.8056	34.6211	31.5957	30.1876	27.5595	25.8452
DB5	61.7426	54.5710	51.3990	47.8194	45.3694	43.2898	41.3464	39.4254	37.3646	35.0922	31.9389	30.5570	29.3886	28.2490

Abbreviation: PSNR, peak signal-to-noise ratio.

5 | CONCLUSION

This study presents a medical image watermarking in the spatial domain using the methods of [30] and [31]. First, the ROI of the MRI images is detected by the automatic scheme presented in [31]. After that, the encoded binarized EPR data are embedded in the RONI. For the extraction of watermark data, assuming that the salt and pepper noise attack from low to very high density has occurred, the ARSPN method is used to decrease the existing noise. This high-performance noise cancellation method increases the quality of attacked images and reduces the data extraction error. The main reason for decreasing BER is the preconditions to extract the watermark data, that is, labeling the noisy pixels of RONI and omitting the information of those pixels. This innovative condition extracts only the healthy data, and BER is increased dramatically. The BER average value for noise density from 0% to 70% is less than 10%, for density 80% to 95% is between 10 and 26.7, and for 97% is 38.6. These results show the high performance of applying the proposed method on the five MRI databases.

AUTHOR CONTRIBUTIONS

Javad Ebrahimnejad: Conceptualization; Data curation; Formal analysis; Investigation; Methodology; Software; Visualization; Writing—original draft; Writing—review & editing. Alireza Naghsh: Conceptualization; Data curation; Formal analysis; Investigation; Methodology; Project administration; Resources; Supervision; Validation; Writing—review & editing. Hossein Pourghasem: Investigation.

FUNDING INFORMATION
No funds, grants, or other support were received.

CODE AVAILABILITY
The codes of this study are available and could be sent to the journal by request.

CONFLICT OF INTEREST STATEMENT
The authors declare no conflict of interest.

DATA AVAILABILITY STATEMENT
The data that support the findings of this study are available from the corresponding author upon reasonable request.

ORCID
Javad Ebrahimnejad https://orcid.org/0000-0003-4831-4546
Alireza Naghsh https://orcid.org/0000-0002-0842-0419

REFERENCES
1. Giri, K.J., Jeelani, Z., Bhat, J.I., Bashir, R.: Survey on Reversible Watermarking Techniques for Medical Images. In: Multimedia Security, pp. 177–198. Singapore: Springer (2021)
2. Thabit, R.: Review of medical image authentication techniques and their recent trends. Multim. Tools Appl. 80(9), 13439–13473 (2021)
3. Elhoseny, M., Ramírez-González, G., Abu-Elnasr, O.M., Shawkat, S.A., Arunkumar, N.: Secure medical data transmission model for IoT-based healthcare systems. IEEE Access (2018) https://doi.org/10.1109/ACCESS.2018.2817615
4. Anand, A., Singh, A.K.: Watermarking techniques for medical data authentication: A survey. Multim. Tools Appl. 80(20), 30165–30197 (2021)
5. Allaf, A.H., Kbir, M.H.A.: Usage of watermarking techniques in medical imaging. In: Proceedings of the 3rd International Conference on Smart City Applications, pp. 1–6 (2018)
6. Navas, K.A., Sasikumar, M.: Survey of medical image watermarking algorithms. In: Proceedings of the Internation Conference Sciences of Electronics, Technologies of Information and Telecommunications, pp. 25–29 (2007)
7. Eswaraiah, R., Reddy, E.S.: A fragile ROI-based medical image watermarking technique with tamper detection and recovery. In: 2014 Fourth International Conference on Communication Systems and Network Technologies, IEEE, pp. 896–899 (2014)
8. Ali, M., Ahn, C.W.: An optimal image watermarking approach through cuckoo search algorithm in wavelet domain. Int. J. Syst. Assur. Eng. Manag. 9(3), 602–611 (2018)
9. Shekaramiz, K., Naghsh, A.: Embedding and extracting two separate images signal in salt & pepper noises in digital images based on watermarking. In: 2017 3rd International Conference on Pattern Recognition and Image Analysis (IPRIA), IEEE, pp. 32–37 (2017)
10. Kumar, C., Singh, A.K., Kumar, P.: Improved wavelet-based image watermarking through SPIHT. Multim. Tools Appl. 79(15), 11069–11082 (2020)
11. Singh, A.K.: Improved hybrid algorithm for robust and imperceptible multiple watermarking using digital images. Multimed Tool Appl. 76(6), 8881–8900 (2017)
12. Hurrah, N.N., Parah, S.A., Sheikh, J.A.: A secure medical image watermarking technique for e-healthcare applications. In: Handbook of Multimedia Information Security: Techniques and Applications, pp. 119–141. Springer: Cham (2019)
13. Gull, S., Loan, N.A., Parah, S.A., Sheikh, J.A., Bhat, G.M.: An efficient watermarking technique for tamper detection and localization of medical images. J. Ambient Intell. Hum. Comput. 11(5), 1799–1808 (2020)
14. Swaraja, K.: Medical image region-based watermarking for secured telemedicine. Multim. Tools Appl. 77(21), 28249–28280 (2018)
15. Zhang, Z., Wang, C., Zhou, X.: Image watermarking scheme based on Arnold transform and DWT-DCT-SVD. In: Signal Processing (ICSP), IEEE 13th International Conference on Signal Processing (ICSP), Chengdu, China (2016)
16. Shehab, A., Elhoseny, M., Muhammad, K., Sangaiah, A.K., Yang, P., Huang, H., Hou, G.: Secure and robust fragile watermarking scheme for medical images. IEEE Access 6, 10269–10278 (2018)
17. Konyar, M.Z., Öztürk, S.: Reed Solomon coding-based medical image data hiding method against salt and pepper noise. Symmetry 12(6), 899 (2020)
18. Shaji, C., Sam, I.S.: Two level data encoding approach for reversible data hiding in dual Stego images. Multim. Tools Appl. 79(37), 26969–26993 (2020)
19. Deeba, F., Kun, S., Dharejo, F.A., Memon, H.: Digital image watermarking based on ANN and least significant bit. Inf. Secur. J Glob. Perspect. 29(1), 30–39 (2020)
20. Vedhanayagam, M.V., Masilamani, V.: A novel image scaling based reversible watermarking scheme for secure medical image transmission. ISA Trans. 108, 269–281 (2021)
21. Zarrabi, H., Hajabdollahi, M., Soroushmehr, S.R., Karimi, N., Samavi, S., Najarian, K.: Reversible image watermarking for health informatics systems using distortion compensation in wavelet domain. In: 2018 40th Annual International Conference of the IEEE Engineering in Medicine and Biology Society (EMBC), IEEE, pp. 798–801 ((2018)
22. Ajili, S., Hajjaji, M.A., Mtibaa, A.: Crypto-watermarking algorithm using weber's law and aes: A view to transfer safe medical image. Sci. Program. 2021, 5559191 (2021)
23. Dagadu, J.C., Li, J.: Context-based watermarking cum chaotic encryption for medical images in telemedicine applications. Multim. Tools Appl. 77(18), 24289–24312 (2018)
24. Parah, S.A., Sheikh, J.A., Ahad, F., Loan, N.A., Bhat, G.M.: Information hiding in medical images: A robust medical image watermarking system for E-healthcare. Multim. Tools Appl. 76(8), 10599–10633 (2017)
25. Liu, J., Ma, Y., Li, S., Lian, J., Zhang, X.: A new simple chaotic system and its application in medical image encryption. Multim. Tools Appl. 77(17), 22787–22808 (2018)
26. Soualmi, A., Alti, A., Laouamer, L.: A novel blind medical image watermarking scheme based on Schur triangulation and chaotic sequence. Concurr. Comput. Pract. Exp. 34(1), e6480 (2021)
27. Salimi, L., Haghighi, A., Fathi, A.: A novel watermarking method based on differential evolutionary algorithm and wavelet transform. Multim. Tools Appl. 79(17), 11357–11374 (2020)
28. Han, B., Jhaveri, R., Wang, H., Qiao, D., Du, J.: Application of robust zero-watermarking scheme based on federated learning for securing the healthcare Data. IEEE J. Biomed. Health Informatics. 27(2), 804–813 (2023)
29. Lee, H.Y.: Adaptive reversible watermarking for authentication and privacy protection of medical records. Multim. Tools Appl. 78(14), 19663–19680 (2019)
30. Ebrahimnejad, J., Naghsh, A.: Adaptive removal of high-density salt-and-pepper noise (ARSPN) for robust ROI detection used in watermarking of MRI images of the brain. Comput. Biol. Med. 137, 104831 (2021)
31. Mousavi, S.M., Naghsh, A., Manaf, A.A., Abu-Bakar, S.A.R.: A robust medical image watermarking against salt and pepper noise for brain MRI images. Multim. Tools Appl. 76(7), 10313–10342 (2017)
32. Sinhal, R., Jain, D.K., Ansari, I.A.: Machine learning based blind color image watermarking scheme for copyright protection. Pattern Recognit. Lett. 145, 171–177 (2021)

How to cite this article: Ebrahimnejad, J., Naghsh, A., Pourghasem, H.: A robust watermarking approach against high-density salt and pepper noise (RWSPN) to enhance medical image security. IET Image Process. 18, 116–128 (2024). https://doi.org/10.1049/ipr2.12937